Quaternary Geochronology 21 (2014) 90–103

Contents lists available at SciVerse ScienceDirect

Quaternary Geochronology

journal homepage: www.elsevier.com/locate/quageo

Research paper

A high-precision $^{40}Ar/^{39}Ar$ age for the Young Toba Tuff and dating of ultra-distal tephra: Forcing of Quaternary climate and implications for hominin occupation of India

Darren F. Mark [a,*], Michael Petraglia [b], Victoria C. Smith [b], Leah E. Morgan [a], Dan N. Barfod [a], Ben S. Ellis [c], Nick J. Pearce [d], J.N. Pal [e], Ravi Korisettar [f]

[a] NERC Argon Isotope Facility, Scottish Universities Environmental Research Centre, Rankine Avenue, East Kilbride, Scotland G75 0QF, UK
[b] Research Laboratory for Archaeology and the History of Art, University of Oxford, Oxford OX1 3QY, UK
[c] Institute of Geochemistry and Petrology, Department of Earth Sciences, ETH Zurich, Clausiusstrasse 25, 8092 Zürich, Switzerland
[d] Institute of Geography and Earth Sciences, Aberystwyth University, Aberystwyth, Ceredigion SY23 3DB, UK
[e] Department of Ancient History, Culture and Archaeology, University of Allahabad, Uttar Pradesh, India
[f] Department of History and Archaeology, Karnatak University, Dharwad 580 003, India

ARTICLE INFO

Article history:
Received 9 June 2012
Received in revised form
22 November 2012
Accepted 11 December 2012
Available online 11 January 2013

Keywords:
Toba
Tephra
$^{40}Ar/^{39}Ar$
Son Valley
Jurreru Valley
Hominin
Climate

ABSTRACT

A new high-precision inverse isochron $^{40}Ar/^{39}Ar$ age for the youngest Toba super-eruption is presented: 75.0 ± 0.9 ka (1 sigma, full external precision, relative to the optimisation model of Renne et al., 2010, 2011). We present the most accurate and robust radio-isotopic age constraint for the Young Toba Tuff. $^{40}Ar/^{39}Ar$ ages for biotite shards harvested from ultra-distal Toba tephra deposits (>2500 km) preserved in archaeological sites in the Middle Son Valley and Jurreru Valley, India, establish provenance with the young Toba super-eruption. The air-fall tephra at these sites can be used as an isochronous horizon facilitating stratigraphic and temporal correlation throughout India. The high-precision $^{40}Ar/^{39}Ar$ age for the young Toba tephra can serve as a tie point for linking of the multiple Greenland ice cores beyond the *GICC05* timescale, and permits correlation to other absolutely dated palaeoclimate archives for the testing of synchronicity in the response of the global climate system.

1. Introduction

The Toba volcano located in northern Sumatra, Indonesia (Fig. 1), is the largest known Quaternary caldera. The caldera (as visible today) extends over 2270 km^2 and is the product of the young Toba super-eruption. The super-eruption produced approximately 2800 km^3 of pyroclastic ejecta (2400 km^3 of dense rock equivalent) (Chesner, 1998; Mason et al., 2004; Matthews et al., 2012), a volume of comparable size to the largest Yellowstone super-eruption (Huckleberry Ridge Tuff; Ellis et al., 2012), but dwarfing other Quaternary eruptions (Fig. 2), including the 1815 eruption of Tambora. Ash fall from the young Toba super-eruption covered approximately 40,000,000 km^2 of South and South-East Asia (Chesner et al., 1991) (Fig. 1). The young Toba tephra (or tuff) (YTT) can be found preserved in marine cores (e.g., ODP 758) throughout the Pacific Ocean, Bay of Bengal and Indian Ocean. Astronomical tuning suggests an age for the eruption of *c.* 73 to 74 ka (Ninkovich, 1979; Oppenheimer, 2002) supporting the radio-isotopic $^{40}Ar/^{39}Ar$ age of 73 ± 4 ka[1] (relative to Fish Canyon Tuff sanidine [FCs] at 27.84 Ma; Chesner et al., 1991).

Despite the large magnitude of the young Toba super-eruption, its impact on both the regional and global climate systems remains controversial with polarised interpretations. Geochemical evidence from ice core records support a hypothesis of substantial impact (Rampino and Self, 1992, 1993; Zielinski et al., 1996; Ambrose, 1998; Rampino and Ambrose, 2000; Williams, 2012b), whilst evidence from sea surface temperature estimates, mammal and termite survival, and archaeological artefacts support a hypothesis of

* Corresponding author. Tel.: + 44 (0) 1355 270194; fax: + 44 (0) 1355229898.
E-mail address: D.Mark@suerc.gla.ac.uk (D.F. Mark).

[1] $^{40}Ar/^{39}Ar$ age ± analytical uncertainty here and throughout (unless otherwise stated) are reported at the 1σ (68%) confidence level.

1871-1014/$ – see front matter © 2013 Elsevier B.V. All rights reserved.
http://dx.doi.org/10.1016/j.quageo.2012.12.004

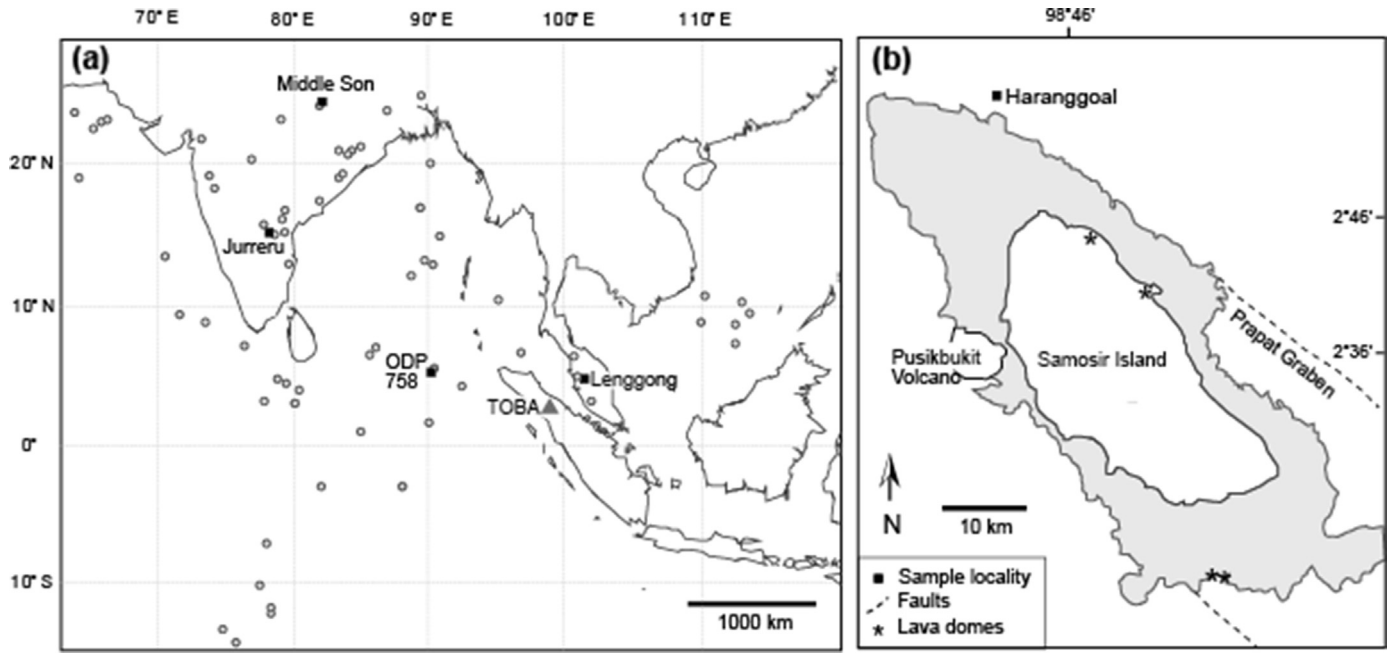

Fig. 1. (a) Map showing the location of the Toba caldera, the sample sites in India (Middle Son Valley and Jurreru Valley) and other locations where Toba tephra is found (circles) (modified from Oppenheimer, 2002; Jones, 2010). (b) The Toba caldera as visible today and the sampling location at Haranggoal (modified from Smith et al., 2011a).

minimal impact (Schulz et al., 2002; Petraglia et al., 2007; Louys, 2012). Some researchers have viewed the Toba super-eruption as one of the most significant events in the course of human evolution, leading to cataclysmic changes in terrestrial ecosystems and the near extinction of our species (Ambrose, 1998; Rampino and Ambrose, 2000; Williams et al., 2009). Genetic evidence has been used to suggest a sudden drop in the numbers of the ancestors of living human populations to a few thousand at *c.* 74 ka (Haigh and Maynard Smith, 1972; Harpending et al., 1993; Jorde et al., 1998), with survivors concentrated solely in African biotic refugia (Tishkoff et al., 2009). According to these catastrophic hypotheses, modern humans migrated to Asia and Europe following the young Toba super-eruption, eventually arriving in Australia by *c.* 50 ka (Bowler et al., 2003) and western Eurasia by *c.* 45 ka (Richter et al., 2008). However, the timing of expansion from Africa to Asia relative to the young Toba super-eruption, as well as its direct impact on human populations, has been strongly contested (Gathorne-Hardy and Harcourt-Smith, 2003; Scholz et al., 2007; Cohen et al., 2007).

The potential occurrence of YTT as an isochronous marker horizon across the peninsula of India has sparked debate about the severity of environmental change and the survivorship of foraging

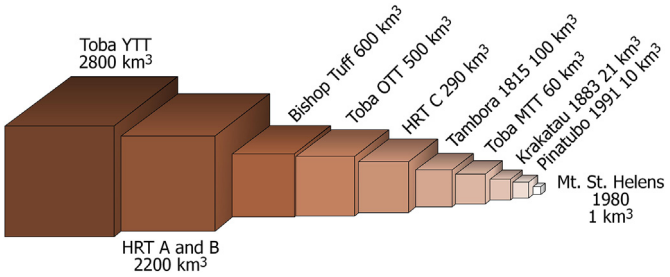

Fig. 2. Eruption volumes for selected Quaternary volcanoes (bulk rock estimates). Volumes are from Chesner and Rose (1991) for Toba (YTT, MTT and OTT), HRT is Huckleberry Ridge Tuff, Yellowstone (Ellis et al., 2012), Bishop Tuff from Hildreth and Wilson (2007), Tambora (Self et al., 2004), Krakatau (Carey et al., 1996), Pinatubo (Scott et al., 1996) and Mt. St. Helens (Sarna-Wojcicki et al., 1981).

populations (Haslam and Petraglia, 2010; Petraglia et al., 2012). The accurate identification and age of terrestrial deposits of ash is therefore critical for evaluating the climatic and environmental effects of the super-eruption and the dispersal and continuity of hominins in Eurasia.

Here we provide a new high-precision $^{40}Ar/^{39}Ar$ age constraint for the youngest Toba super-eruption. We also provide a methodology for $^{40}Ar/^{39}Ar$ dating of ultra-distal-tephra and investigate the ages of tephra located at archaeological sites across India with an aim to establish tephra provenance. The impacts of the young Toba super-eruption on both the local and global climate are discussed, and implications for the evolution of hominin populations are explored.

2. The Toba caldera and distal tephra in India

The Toba Caldera is the product of subduction of the Indian–Australian Plate beneath the Southeast-Asian Plate. Three main eruptive events define the history of one of the largest and most explosive volcanoes on Earth: the young Toba super-eruption (producing the YTT, *c.* 74 ka), Middle Toba eruption (producing the Middle Toba Tuff, MTT, *c.* 500 ka), and the old Toba super-eruption (producing the Old Toba Tuff, OTT, *c.* 790 ka) (Chesner and Rose, 1991; Chesner et al., 1991). At proximal locations on Sumatra each of these deposits are hundreds of metres thick, welded and crystal rich (up to 40%, containing mineral assemblages dominated by quartz, sanidine, plagioclase, biotite and amphibole) (Chesner, 1998). Below the deposits that record explosive volcanism on Sumatra is the Haranggoal Dacite Tuff (HDT, *c.* 1200 ka; Chesner and Rose, 1991) and a series of andesites (*c.* 1300 ka; Yokoyama and Hehanussa, 1981).

Distally, tephra from the Toba eruptions has been documented in Malaysia (Scrivenor, 1930), the Bay of Bengal (Ninkovich et al., 1978), the East China Sea (Lee et al., 2004), the Indian Ocean (Pattan et al., 2001), and sites across the peninsula of India (Westgate et al., 1998). The general NW distribution of Toba tephra (Fig. 1) is clearly a result of eruption magnitude and wind direction.

YTT and OTT, products of the two Toba super-eruptions are orders of magnitude larger than MTT, and thus were further reaching than MTT (Chesner and Rose, 1991, Figs. 1 and 2). There has been much discussion about which tephra (OTT or YTT) is present across the peninsula of India but in order for the tephra to be used as an isochronous marker horizon for stratigraphic and temporal correlation, knowledge of the tephra provenance and its age are critical.

Acharyya and Basu (1993) concluded that all tephra deposits across India were YTT and as such, these units provide a unique marker horizon permitting correlation. Mishra and Rajaguru (1994) suggested the young age assignment was at odds with Lower Palaeolithic artefacts associated with the Bori tephra and as such, multiple Toba tephra deposits of various ages must be preserved across India. Westgate et al. (1998) reported glass shard geochemistry from sites in India supporting the conclusion that the tephra distributed across India is YTT. However, it should be noted that glass shard chemistry from the different Toba tephra is similar and whereas tephra correlation to Toba is possible, correlation to specific eruptions is more problematic. Westgate et al. (1998) also presented two fission track ages of 121 ± 22 ka and 84 ± 16 ka from glass shards, both significantly younger than the OTT, the latter overlapping at the 1 sigma confidence level with the age of YTT (Chesner et al., 1991).

Although Acheulean artefacts are found in association with the tephra horizon in India, researchers have suggested that the use of Lower Palaeolithic artefacts in the Late Pleistocene was unlikely (Jones and Pal, 2009). Indeed, it has been noted that for the majority of locations in India, the stratigraphic association between tephra and artefacts is problematic and poorly documented (Jones, 2007).

Through $^{40}Ar/^{39}Ar$ dating of volcanic glass Westaway et al. (2011) favour correlation of the tephras across India with OTT. However, there are statistical issues with the selection criteria for age steps and 'plateaus' (single steps through to four steps, totalling a maximum of 20–30% ^{39}Ar) from highly discordant and continuously changing $^{40}Ar/^{39}Ar$ age spectra (step-heating of distal glass). This contribution does not conform to the best practices adopted widely in the $^{40}Ar/^{39}Ar$ community (e.g., see discussion in Renne et al., 2009).

Smith et al. (2011a), realising the difficulty in resolving OTT and YTT using glass shard chemistry, performed geochemical analyses on the biotite. The data indicate that owing to subtle differences in biotite geochemistry, tephra from sampled sites across India could indeed be directly correlated with YTT.

Currently there is a discrepancy between the stratigraphic observations, tephra geochemistry, and the archaeology and above ash correlations. Hence, we have sampled tephra from key sites in an attempt to resolve the two-decade old question of 'which Toba tephra is preserved at various archaeological sites throughout India?'

3. Sample sites

Tuffs both proximal (Sumatra) and distal (across India) to the Toba Caldera were collected. The proximal samples were collected to facilitate determination of a high-precision $^{40}Ar/^{39}Ar$ age for YTT. Distal samples were collected to allow establishment of a definitive provenance (and an age) for the primary ash fall horizons at archaeological sites in India.

3.1. Proximal deposits

The YTT proximal sample was collected at Haranggoal, near the northern tip of the caldera (Figs. 1 and 3). Four sub-units are observed in the YTT deposit (Knight et al., 1986). We sampled (sample NP8, 2°53′11″N, 98°39′41″E) from the base of YTT, the second sub-unit, at ~1220 m above sea level (m asl) and ~325 m above the lake surface. The basal YTT unit is 20 m thick, pumice-rich, slightly welded, lithic and crystal-rich, inversely graded tuff with pumice clasts that are ~7 cm in diameter. Knight et al. (1986) provide a full description of the units at Haranggoal. The sampled unit is overlain by a ~20 m thick, pumice-rich zone with large clasts (10–20 cm in diameter) in a crystal-rich matrix. It is overlain by a ~20 m-thick lithic-rich unit containing clasts of welded tuff and argillite, with large pumices (10–20 cm in diameter) in a fines-poor, crystal-rich matrix. The rest of the YTT unit at this site, >100 m, is comprised of a white-grey non-welded tuff, with pumices up to 63 cm in a crystal- and lithic-rich matrix (Fig. 3).

3.2. Distal deposits

Distal deposit samples were collected from air-fall tephra horizons below reworked tephra in the Middle Son Valley in northern India (Madhya Pradesh) and the Jurreru Valley in southern India (Andhra Pradesh). These sites were chosen because they preserve primary ash-fall layers (4–5 cm thick) in the basal deposits (Petraglia et al., 2007; Jones, 2010) with black flecks suspected of being small biotite shards. The identification of air-fall deposits was based upon a number of field observational criteria: the unit forms a homogenous, uniformly-bedded deposit which blankets pre-existing topography with only minor variation in thickness locally; the unit shows sharp contrast with underlying sediments and overlying ash deposits; the unit shows no cross bedding features, but may have weakly developed planar bedding; the unit is characterised dominantly by glass shards and the absence of non-volcanic detrital material (Gatti et al., 2011; Blinkhorn et al., 2012; Lewis et al., 2012; Matthews et al., 2012). Particle size analysis has confirmed the difference between the primary and reworked ash deposits (Matthews et al., 2012; Lewis et al., 2012), with a minor contribution of coarse sediments owing to bioturbation. Targeted analysis of the primary ash shows that mean grain size is small (<100 μm) with a total absence of coarser-grained sediments (Lewis et al., 2012).

3.2.1. Middle Son Valley

The Middle Son Valley (Fig. 1) is one of the key terrestrial sites with a long history of geological and archaeological research (Sharma and Clark, 1983; Williams et al., 2006; Jones and Pal, 2009; Petraglia et al., 2012). The Ghoghara section was examined as a part of a new series of excavations in the region. Cultural and palaeo-environmental reconstructions previously assumed that the tephra distributed across the valley had a YTT provenance.

Above the primary air-fall tephra horizon (Fig. 4) there are several metres of reworked tephra, concentrated as a consequence of alluvial processes (Jones, 2010; Lewis et al., 2012; Petraglia et al., 2012). Chronometric ages (OSL) have been obtained for the alluvial deposits within the valley (Williams et al., 2006), although studies disagree on the stratigraphic position of the ash-fall in the sequence (Jones and Pal, 2009; Jones, 2010). Despite the fact that there is an air-fall tephra at Ghoghara, IRSL dating of this section has produced young ages below the ash (Neudorf et al., 2012). The OSL ages are apparently erroneous and claims that grains have been 'mixed in slump deposits' find no stratigraphic support. Westaway et al. (2011) have suggested the Middle Son Tephra is OTT, which, if true, would necessitate significant revision of geological, environmental, and archaeological data in the region.

We sampled 1 kg of material approximately 1 cm from the base and 1 cm from the top of the primary ash fall horizon (Sample GS1, Rehi-Son confluence, 24°30′7″N, 82°1′2″E). In addition to small (30–100 μm-sized) glass shards, as suspected, the tephra contains small (50–90 μm-sized) shards of biotite.

Sampled unit (NP8, 1220 m above sea level) from massive lapilli tuff near the base of YTT at Haranggoal, Sumatra

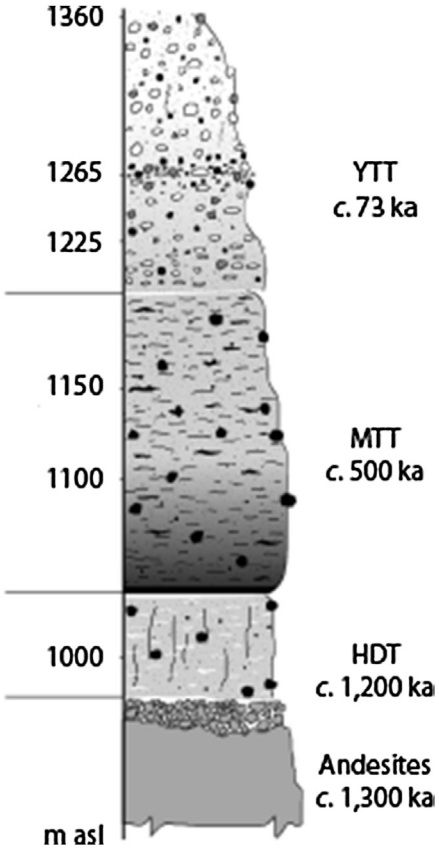

Fig. 3. Proximal Toba YTT deposit at Haranggoal, northeast of the caldera (stratigraphic column modified from Knight et al., 1986). Four YTT sub-units are observed at the site. The sample (NP8) is from the base of the YTT deposit that sits on an unconformity above MTT. Pumice clasts in the photo are ~15 cm in diameter.

3.2.2. Jurreru Valley

The Jurreru Valley (Fig. 1) preserves large quantities of buried ash that are exposed as a result of modern quarrying. Surveys have identified a range of archaeological sites spanning from the Acheulean into the historic period (Blinkhorn et al., 2010; Shipton et al., 2010). A stratigraphic and geomorphological framework for the Jurreru River Valley has been constructed (Petraglia et al., 2012). The river bottom preserves a long sequence of sedimentary deposits, including a tephra deposit, which forms a distinct marker horizon. The tephra varies between 1 and 2.5 m thick and extends over several kilometres. Notable is the presence of a thin (approximately 4 cm) basal primary air-fall tephra unit found above palaeosols (Petraglia et al., 2007; Jones, 2010; Blinkhorn et al., 2012; Matthews et al., 2012). Above the thin primary air-fall tephra layer (Fig. 5), is again a thick horizon of reworked tephra, a function of the rivers concentrating ash from the landscape. Middle Palaeolithic artefacts occur below and above the ash and in deposits as young as 38 ka (Petraglia et al., 2012).

OSL results from Jwalapuram Locality 3 produced an age of 77 ± 6 ka below the ash and 74 ± 7 ka in sands and silts above the ash bed (Petraglia et al., 2007). The below ash ages have been supported by an OSL age of 71 ± 8 ka at Jwalapuram Locality 22 (Haslam et al., 2012). An OSL dating programme resulted in reconsideration of the single above-ash age at Jwalapuram Locality 3, with new data suggesting an age no earlier than 55 ka (Balter, 2010; Roberts et al., 2010), although this conclusion is at odds with stratigraphic observations and the presence of ash-rich silts immediately overlying the thick reworked ash deposits.

We sampled greater than 1 kg of material (Sample 16-1E-B2, JV7, 15°19′2″N, 78°7′59″E) from the interior portion of the ash-fall tephra (i.e., away from base and reworked material above). Glass shards dominate the ash and small black flecks were confirmed as 50–80 μm-sized shards of biotite.

4. Methods

The dating of proximal YTT utilised a standard analytical approach owing to the presence of large crystals of sanidine and biotite (e.g., Mark et al., 2010; Ellis et al., 2012). The analytical challenge for this project was the preparation and dating of the distal YTT deposits. Although the distal samples contain abundant K-bearing glass shards, volcanic glass shards have been shown (e.g., Morgan et al., 2009) to provide unreliable $^{40}Ar/^{39}Ar$ ages likely due to a combination of post eruption K-loss (potentially due to glass hydration) and ^{37}Ar and ^{39}Ar recoil effects. These effects are amplified by a high surface area to volume ratio of glass shards and thus short effective diffusion dimensions (radii of glass shards) (Morgan et al., 2009).

4.1. Sample preparation

Samples were prepared at the Scottish Universities Environmental Research Centre (SUERC). Detailed methodology for preparation of the proximal samples can be found in Mark et al. (2011a) and we present a brief summary. An in-depth discussion of the methodology utilised for the preparation of the distal samples is presented below.

4.1.1. Proximal samples

Samples of pumice collected from the proximal samples were crushed to cm-sized clasts using a jaw crusher. A disc mill was used to disaggregate material and concentrate crystal sizes between 500

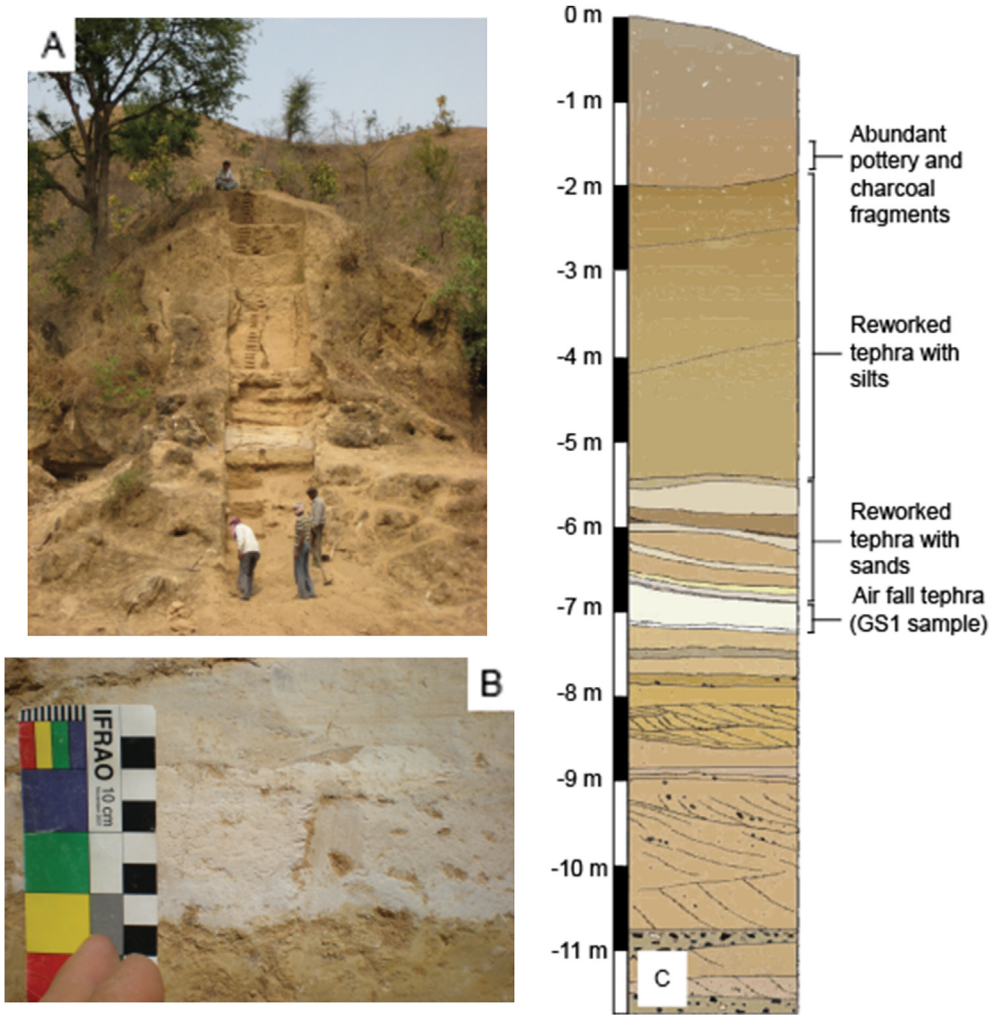

Fig. 4. Stratigraphy at the Middle Son Valley site, India. (A) Excavation at the Ghoghara locality. Note the white ash bed in section. (B) Basal ash layer at Ghoghara identified as an air-fall deposit (*c*. 5 cm thick), overlying the brown clay and underlying the medium to coarse grained reworked ash. Small bioturbation features are present (Lewis et al., 2012). (C) Stratigraphic log of the Ghoghara section. Note location of sample GS1. Photos P. Ditchfield.

and 1500 μm. Samples were washed, sieved and magnetically separated to produce two aliquots, one concentrated in feldspar and the other concentrated in biotite. Sanidine (1000–1500 μm) was handpicked under a binocular microscope using the methods of Hynek et al. (2010) to ensure a pure separate. After leaching in dilute HF and rinsing in de-ionised water and methanol, the grains were parcelled into Cu packets and positioned within an Al holder for irradiation. Inclusion free biotite was handpicked (1000–1500 μm) under binocular microscope. The biotite was cleaned in methanol and de-ionised water, parcelled into Cu packets and positioned within an Al holder for irradiation.

4.1.2. Distal samples

Distal tephra samples were disaggregated gently using a vibrating plate and pestle and mortar. Samples were sieved and washed using de-ionised water. The 63–125 μm size fraction was selected due to the highest concentration of biotite shards and because Paine et al. (2006) and Vanlaningham and Mark (2011) demonstrated that biotite crystals sufficiently large, >50 μm and >63 μm, respectively, show no evidence of ^{37}Ar and ^{39}Ar recoil. Magnetic separation was used to concentrate the biotite shards and under binocular microscope contaminating material (as well as biotite shards with adhering glass) was removed by hand picking. Relative to the glass shards that showed evidence of extensive alteration, the biotite was pristine, supporting the observations of Smith et al. (2011a). From over 1 kg of material from the two sample sites, approximately (allowing for weighing of small amounts of material) 0.02 g of material was harvested from each sample. The biotite crystals were cleaned in methanol and de-ionised water. The biotite from both samples was divided into 15 aliquots (approximately 0.001 g biotite per aliquot) for $^{40}Ar/^{39}Ar$ dating. Aliquots were parcelled into Cu packets and positioned within an Al holder for irradiation.

4.2. $^{40}Ar/^{39}Ar$ analytical approach and data handling

International standard Alder Creek Tuff sanidine (ACs, 1.193 ± 0.001 Ma; Nomade et al., 2005), a secondary standard referenced against the Fish Canyon sanidine age (FCs) (28.02 ± 0.16 Ma) of Renne et al. (1998), was loaded adjacent to the samples of unknown age. Samples were irradiated for 0.08 h in the Cd-lined RODEO facility of the McMaster reactor. ACs grains (n = 20 per disc) were analysed by total fusion with a focused CO_2 laser. The J-parameter was determined to a precision of *c*. 0.25%. Both FCs and Taylor Creek Rhyolite sanidine (TCR-2s) were also loaded adjacent to the Toba tephra samples to check J-parameter accuracy. Using J-parameter

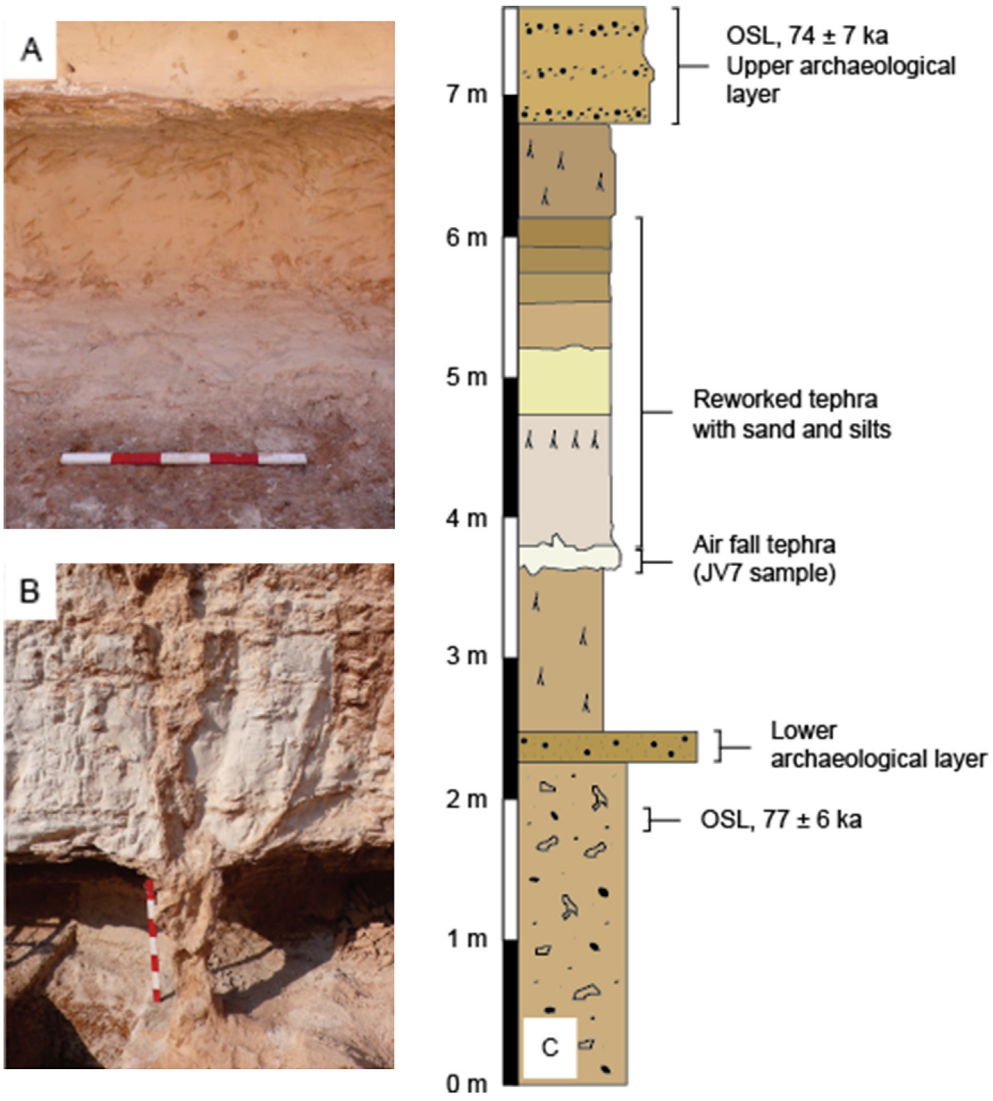

Fig. 5. Stratigraphy in the Jurreru Valley, India. (A) Basal tephra layer of air-fall ash at contact with underlying sediments (JV7), overlain by reworked ash. Note horizontal lithified clay horizon in reworked ash (scale bar 50 cm). (B) Fossilised tree trunk with branching structure in YTT deposit (Blinkhorn et al., 2012). (C) Stratigraphic log of Jwalapuram locality. Note the location and context for sample JV7 (after Petraglia et al., 2007). Photos A. Durant.

measurements from ACs, both FCs and TCR-2s yield ages that overlap with those defined by Renne et al. (1998) indicating appropriate measurements of the J-parameter from ACs for the determination of unknown ages.

Single grains of sanidine (>1000 μm diameter) and biotite (thick packets of mica sheets, >1000 μm diameter) from the proximal samples, and distal biotite aliquots (multi-grain, 0.001 g populations) were loaded into Cu planchettes in ultra-high vacuum laser cells with doubly pumped ZnSe windows. A heat lamp held at 100 °C was used to bake splits of the distal samples at ultra-high-vacuum for two different prolonged durations (17 and 21 days for the two different samples) owing to the large surface area of the small crystals. The difference in bake duration was to allow for quantitative testing of any Ar loss from the fine-grained material induced by the bake. Proximal samples were baked at 100 °C for only 3 days at ultra-high-vacuum. Using a CO_2 laser, the sanidine crystals were first degassed at low temperature (defocused laser beam, 0.3 W) prior to total fusion. Radiogenic ^{40}Ar ($^{40}Ar^*$) yields were thus improved (several gas aliquots were analysed following degassing) whilst no ^{39}Ar was liberated during the degassing step. Biotite crystals were not degassed at low temperature as significant ^{39}Ar was liberated following initial experimentation. Biotite crystals were fused using a CO_2 laser.

All gas fractions were subjected to 180 s of purification with two SAES GP50 getters (one at room temperature, the other at 450 °C) and a cold finger maintained at −95.5 °C using a mixture of dry ice ($CO_{2[s]}$) and acetone. Argon isotope ratios (i.e., ion beam intensities) were measured using a MAP 215-50 mass spectrometer in peak jumping mode. The mass spectrometer has a measured sensitivity of 1.13×10^{-13} mol/volt. Both the extraction and clean-up processes were automated, as were the mass spectrometer peak jumping routines and data acquisition. For the proximal samples full system blanks were measured after every two analyses of unknowns. We required improved blank control for the distal samples and full system blanks were run after every single analysis (unknown and calibration). Average full system blanks ± standard deviation ($n = 129$) from the entire run sequence were used to correct raw isotope measurements of unknowns. Owing to the small amounts of material from the distal samples, some ^{40}Ar measurements were less than a factor of ten times larger than full system blank measurements. Mass discrimination was monitored by analysis of air pipettes after every five analyses ($n = 41$). The Argon isotope data

were corrected for backgrounds, mass discrimination, and reactor-produced nuclides and processed using standard data reduction protocols. The decay constants of Steiger and Jäger (1977) and atmospheric argon ratios of Lee et al. (2006), the latter independently verified by Mark et al. (2011b), were employed.

The BGC software *MassSpec* was used for data regression. Data are displayed on ideograms and isotope correlation plots (inverse isochron plots). The standard error on the mean (SEM) was determined for all samples that displayed a Gaussian (normal) distribution with a mean square weighted deviation (MSWD) < 1. The SEM $\times$ MSWD$^{1/2}$ used for samples that displayed a Gaussian (normal) distribution with a MSWD > 1. The software was setup to filter data for xenocrysts or detrital contamination – any Ar/Ar age >1.5 Median Absolute Deviations (*n*MADs) from the weighted mean to be rejected from the age calculations. Data were not rejected on the basis of %^{40}Ar*. Using these criteria no data from all runs (for both proximal and distal samples) were rejected.

5. Results

Fig. 6 shows the proximal sanidine and biotite ^{40}Ar/^{39}Ar age data and Fig. 7 shows the distal biotite ^{40}Ar/^{39}Ar age data from both Jurreru Valley and Middle Son Valley. Raw ^{40}Ar/^{39}Ar data are presented in the online supplementary information (SI#1) along with reactor production ratios, background measurements and mass discrimination factors.

The YTT sanidine measurements yield a normal distribution with an age (weighted mean) of 74.2 $\pm$ 0.9 ka (MSWD 0.6, $n = 34$) (Fig. 6). Data cast on an isotope correlation plot define a binary mixing line between initial trapped components of atmospheric composition (Lee et al., 2006) and K-correlated radiogenic component whose age is indistinguishable at the 1 sigma confidence level with the weighted mean age for the population (Fig. 6). The YTT biotite also yields a normal distribution with a weighted mean age (72.6 $\pm$ 7.2 ka, MSWD 0.3, $n = 26$, Fig. 6) that is significantly less precise than, but indistinguishable from the YTT sanidine age. Low radiogenic ^{40}Ar (^{40}Ar*) yields (typically less than 8% ^{40}Ar*) are diagnostic of the proximal biotite and responsible for the large spread in data compared to the sanidine ages. Data plotted on an isotope correlation plot (Fig. 6) define an isochron with initial trapped component overlapping with atmospheric ^{40}Ar/^{36}Ar (Lee et al., 2006) and a radiogenic age component that is indistinguishable from the weighted mean age.

The Jurreru Valley distal biotite defines a slightly skewed (asymmetric) bell-shaped (normal) distribution with a weighted mean age of 73.9 $\pm$ 4.4 ka (MSWD 0.7, $n = 15$, Fig. 7). The data define an isochron on an isotope correlation plot (Fig. 7) that has an initial trapped component that overlaps with accepted atmospheric

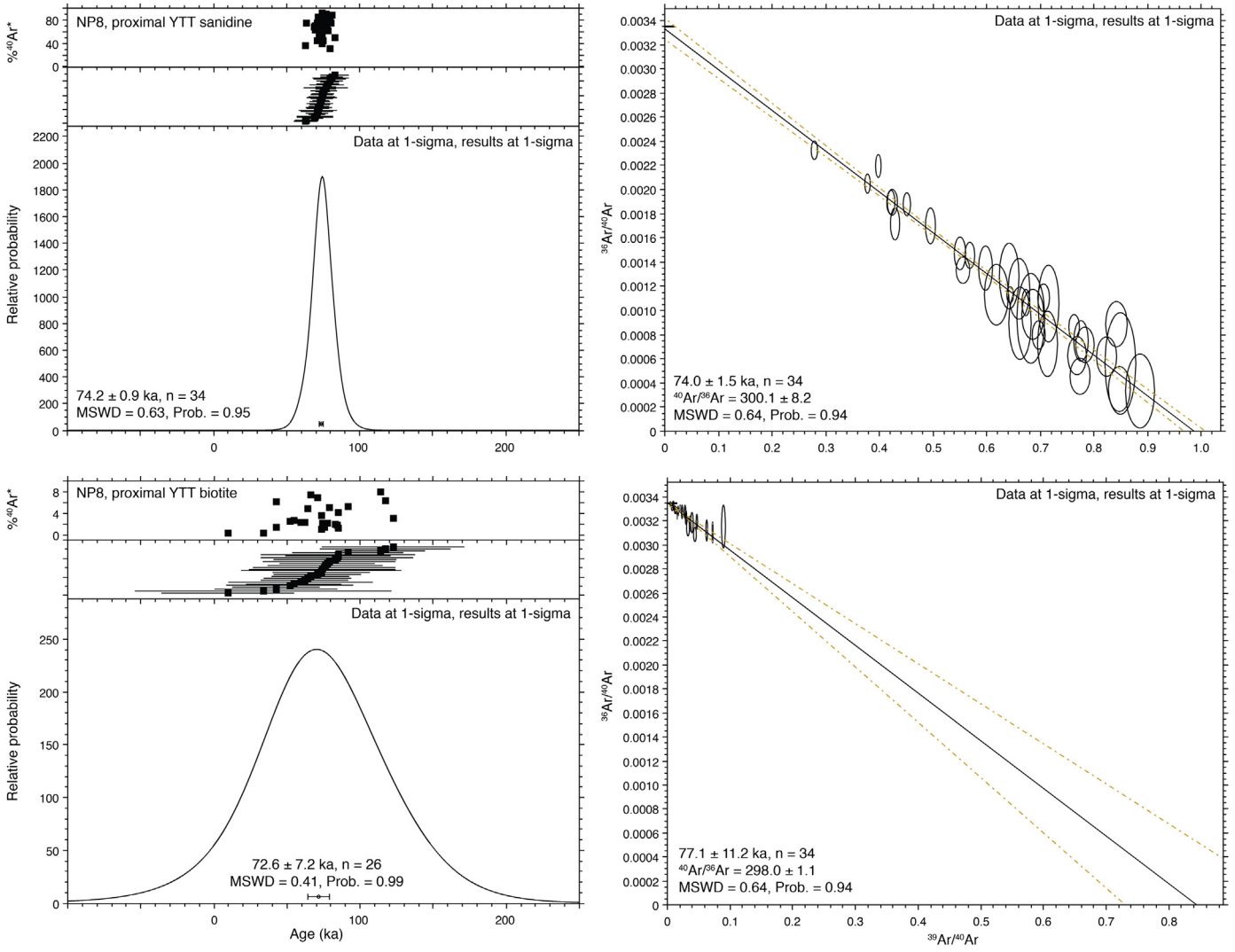

Fig. 6. ^{40}Ar/^{39}Ar age data plotted on ideogram and isotope correlation plots for the proximal samples (Haranggoal, sanidine and biotite).

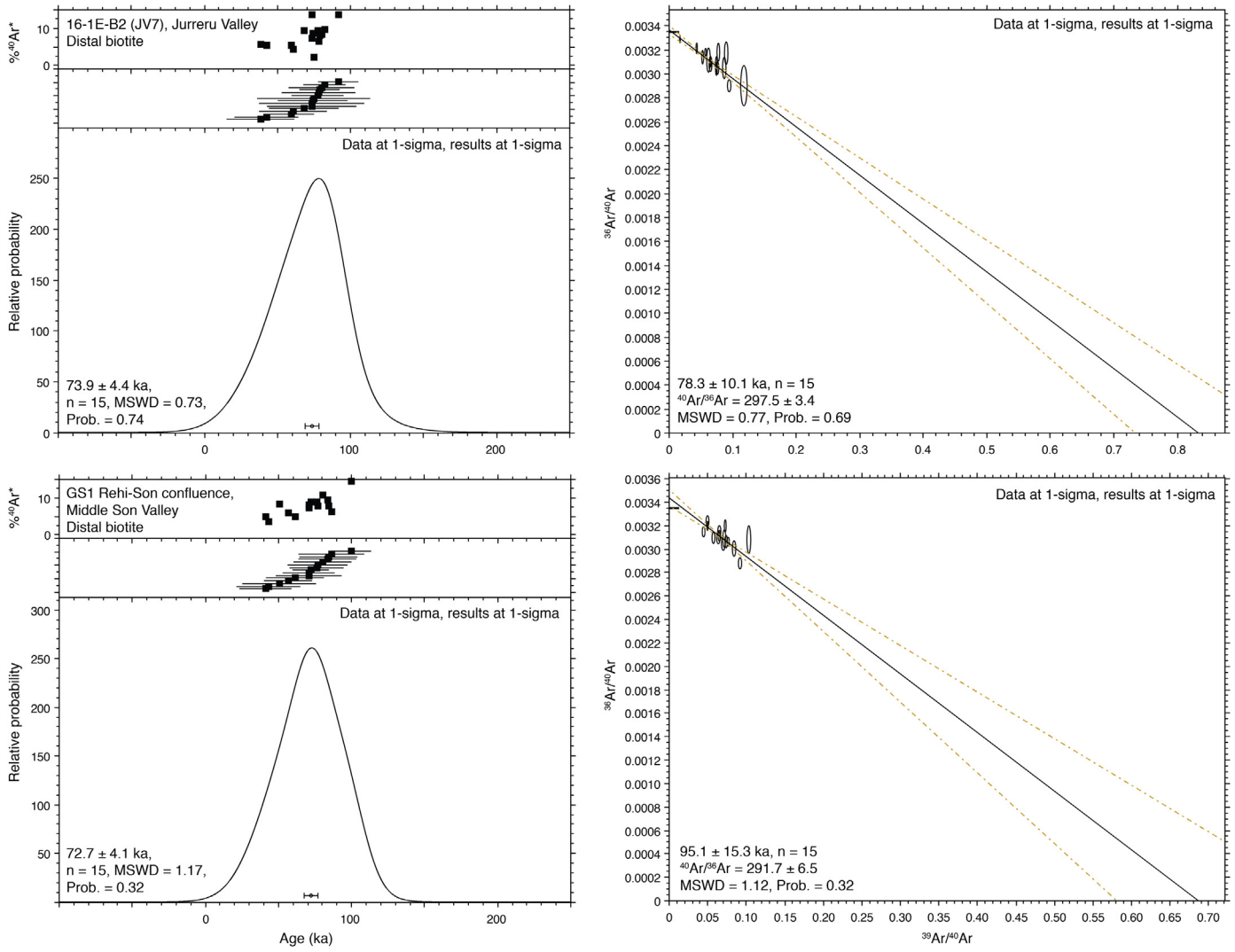

Fig. 7. $^{40}Ar/^{39}Ar$ age data plotted on ideograms and isotope correlation plots for the distal samples (Middle Son Valley and Jurreru Valley, biotite).

$^{40}Ar/^{36}Ar$ (Lee et al., 2006) and an age component that is indistinguishable at the 1 sigma confidence level with the weighted mean age.

The Middle Son Valley distal biotite defines a normal distribution with a weighted mean age of 72.7 ± 4.1 ka (MSWD 1.2, $n = 15$, Fig. 7). The data cast on an isotope correlation plot define an atmospheric trapped $^{40}Ar/^{36}Ar$ component (Lee et al., 2006) but the K-correlated age component does not overlap at the 1-sigma confidence level with the weighted mean age (Fig. 7). This is due to a higher degree of scatter in the Middle Son Valley sample compared to the Jurreru Valley sample, as demonstrated by the increased MSWD. Further, a tighter clustering in $\%^{40}Ar^*$ reduces dispersal along the isochron and results in a larger uncertainty envelope associated with extrapolation of the isochron to the *x*-axis (Fig. 7). The isochron age is however indistinguishable at the 2 sigma confidence level from the weighted mean age.

Following baking of distal samples for two different durations we observed no evidence for laboratory induced Ar loss with reproducible ages for all sample aliquots irrespective of bake duration (Fig. 7). The distal biotite samples surprisingly have greater $^{40}Ar^*$ yields than proximal biotite (Figs. 6 and 7) but relatively poor $^{40}Ar^*$ yields compared to sanidine. With the expectation of greater surface contamination in the fine distal grains and to maximise data quality, the distal biotites experienced an extended bake-out (discussed in Section 4). However, the observed difference between distal and proximal biotite grains may result from differences in laboratory handling and/or from varying depositional processes. For example, following deposition the proximal deposits experienced compaction and welding with heat (up to 200 °C) in thick deposits (>100 m) retained for potentially hundreds of years (Rose and Chesner, 1990). This would imply potential for bulk entrainment and trapping of air into the deposit and an extended cooling history relative to the distal deposits (that would have essentially experienced instantaneous cooling), potentially promoting the proximal biotites to a greater degree of air contamination.

We aim to test this scenario in the near future by treating both proximal and distal samples to the same bake-out procedure (i.e., samples loaded in the same laser cell for analysis). In hindsight, to potentially improve the quality of the proximal biotite data, we should have utilised the same procedure of removing contamination as we did for the distal samples (i.e., extended bake of the laser cell), although this would not guarantee improved $^{40}Ar^*$ yields from the proximal samples if depositional processes were governing the incorporation of atmospheric argon.

No data from either the proximal or distal samples were rejected (either on the basis of xenocryst/detrital contamination or

statistical analysis). All four samples, the proximal sanidine and biotite, the distal biotite from Jurreru Valley and Middle Son Valley, yielded consistent and reproducible $^{40}Ar/^{39}Ar$ ages with varying levels of analytical precision (Figs. 6 and 7). All inverse isochrons defined atmospheric $^{40}Ar/^{36}Ar$ initial trapped components (Figs. 6 and 7) and do not show the presence of significant excess ^{40}Ar.

6. Discussion

6.1. Provenance and age of the ultra-distal tephra deposits in India

The distal biotite age data for both Jurreru Valley and Middle Son Valley (Fig. 7) yield $^{40}Ar/^{39}Ar$ ages that are indistinguishable from the previously reported radio-isotopic $^{40}Ar/^{39}Ar$ age for YTT, 73 ± 4 ka (Chesner et al., 1991), relative to the use of the same standard ages and decay constants (see discussion in Section 6.2). Our data contradict the data of Westaway et al. (2011) who suggest an approximate age of 800 ka (comparable to an OTT age) for tephra throughout the Middle Son Valley. The data supports the work of Smith et al. (2011a) who correlated the distal biotite shards from both sites to the proximal Toba YTT deposits. Based on similar biotite composition and indistinguishable $^{40}Ar/^{39}Ar$ ages for samples from both sites, we show the primary air fall tephra layers at Middle Son Valley and Jurreru Valley, India, which are separated by 1100 km (and >2500 km from Toba), provide an isochronous marker horizon permitting both stratigraphic and temporal correlation with YTT. There is no evidence of an ash layer with an OTT age (i.e., c. 800 ka) preserved at these sites. Given that the YTT eruption was approximately six times larger than the OTT eruption (and approximately 45 times larger than the MTT eruption) (Fig. 2) it is perhaps not surprising that there is no evidence of OTT in such distal localities to the Toba caldera.

Scattered throughout India there are more exposures of air fall ash in river valley cuttings and at excavated archaeological sites (Jones, 2010, Fig. 1). For the Middle Son Valley and the Jurreru Valley we can now have full confidence in using the age of the YTT eruption as a marker horizon. However, owing to poor stratigraphic correlation, the large distances between sites, and the controversial nature of the archaeological assemblages, a more extensive $^{40}Ar/^{39}Ar$ dating programme that adopts the same robust approach outlined here is required to test the hypothesis that more than one distal Toba ash fall event is preserved in India. Certainly the work of Westaway et al. (2011) at other sites (e.g., Bori tephra) requires thorough examination and testing with renewed data collection. Work at the NERC Argon Isotope Facility (SUERC) on the provenance of these deposits is on going.

6.2. Age of the young Toba super eruption (YTT)

Interestingly, it is often noted that coeval $^{40}Ar/^{39}Ar$ ages for sanidine and biotite do not always match due to the presence of extraneous ^{40}Ar in biotite, and its absence in sanidine (e.g., Hora et al., 2010). This is not the case for the YTT. The coeval sanidine and biotite $^{40}Ar/^{39}Ar$ data from the proximal YTT deposit (Fig. 6) have ages that are indistinguishable at 1 sigma uncertainty, with both the sanidine and biotite having initial trapped components that overlap with accepted atmospheric argon ratios (Lee et al., 2006). Therefore the proximal sanidine and biotite data can be used to define a precise radio-isotopic $^{40}Ar/^{39}Ar$ age for the young Toba super-eruption. We have cast all $^{40}Ar/^{39}Ar$ data proximal data (sanidine and biotite) on an isotope correlation plot (i.e., global isochron) to define the most accurate YTT age without making assumptions concerning the initial trapped $^{40}Ar/^{36}Ar$ component (Fig. 8). The combination of the low $^{40}Ar^*$ biotite data and higher $^{40}Ar^*$ yield sanidine data define an isochron with widely dispersed

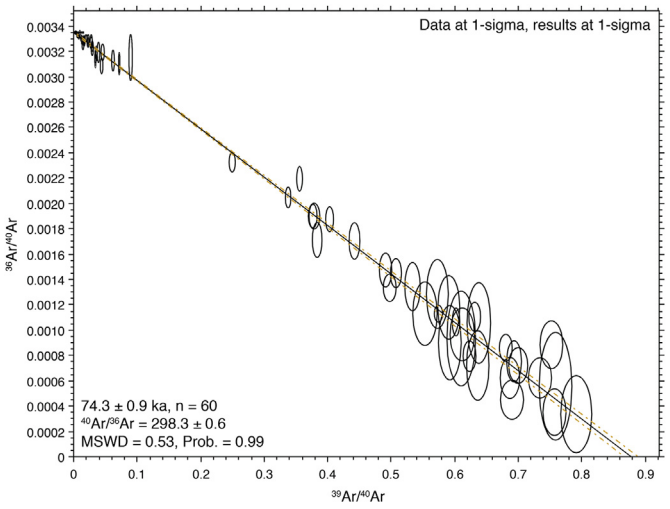

Fig. 8. Isotope correlation plot showing global proximal sample dataset.

data. The data define an initial trapped component of 298.3 ± 0.6 overlapping with the accepted atmospheric $^{40}Ar/^{36}Ar$ of Lee et al. (2006) and an age of 74.3 ± 0.9 ka.

The $^{40}Ar/^{39}Ar$ method is a relative dating technique with all ages referenced back to a standard of known age. Recently Renne et al. (2010, 2011) published an optimisation model that used constraints from ^{40}K activity, K–Ar isotopic data, and pairs of ^{238}U–^{206}Pb and $^{40}Ar/^{39}Ar$ data as inputs for estimating the partial decay constants of ^{40}K and $^{40}Ar^*/^{40}K$ ratio of FCs. This calibration has reduced systematic uncertainties (i.e., improved accuracy) in the $^{40}Ar/^{39}Ar$ system and has yielded an age for FCs that is indistinguishable at the 2-sigma confidence level from the astronomically tuned FCs age of Kuiper et al. (2008).

Therefore, to present an accurate $^{40}Ar/^{39}Ar$ age for the Toba YTT we have recalculated our age relative to the optimisation model of Renne et al. (2010, 2011) using the approach outlined in Ellis et al. (2012). To allow readers to see the impact on the age of the YTT when using the different standard ages and decay constants we have presented the data in this two-step approach: (1) relative to Steiger and Jäger (1977) and Renne et al. (1998) (Fig. 6), and (2) data recalculated relative to Renne et al. (2010, 2011). Note that due to the correlated uncertainties associated with the Renne et al. (2010, 2011) optimisation model, it is not as simple as just plugging revised standard ages and decay constants along with their uncertainties into routine age equations with employment of linear uncertainty propagation – Monte Carlo modelling is required (as discussed by Renne et al., 2011). When calculated relative to the optimisation model of Renne et al. (2010, 2011) our data define an age for the young Toba super-eruption of: 75.0 ± 0.9 ka (1 sigma, full external precision). Note that due to the young age for YTT the data are relatively insensitive to the propagation of decay constant uncertainty. The age and its uncertainty include all sources of error and are hence are directly comparable to all timescales as defined by other chronometers.

During revision of this manuscript Storey et al. (2012) published an age for the YTT of 73.9 ± 0.3 ka (1 sigma, full external precision) referenced against the FCs age of Rivera et al. (2011). The FCs age of Rivera et al. (2011) was calibrated by astronomical tuning of the A1 tephra and is out with 2 sigma uncertainty of the FCs age proposed by Renne et al. (2010, 2011) but, like Renne et al. (2010, 2011) it is within 2 sigma uncertainty of the FCs age of Kuiper et al. (2008). However, new (blindly collected) $^{40}Ar/^{39}Ar$ data collected by The Berkeley Geochronology Centre and The Scottish Universities Environmental Research Centre (Renne et al., in press) for the IrZ

coal bentonite (the stratigraphically closest marker horizon to the paleontologically-defined Cretaceous–Paleogene [K–Pg] boundary) show that whereas both the calibrations of Kuiper et al. (2008) and Renne et al. (2010, 2011) support the choice of 405 ka eccentricity cycles to determine the age of the K–Pg boundary at Zumaya (Kuiper et al., 2008), the calibration of Rivera et al. (2011) places the K–Pg boundary exactly intermediate between two possible choices of 405 ka cycles. Therefore the astronomically tuned age for FCs as proposed by Rivera et al. (2011) is oddly inconsistent with any astronomical age for the K–Pg boundary, casting doubt on the accuracy of the Rivera et al. (2011) study. Providing the K–Pg tuning of Kuiper et al. (2008) is correct (and it has not been challenged in the four years since publication), the $^{40}Ar/^{39}Ar$ calibration of Renne et al. (2010, 2011) is proven to be the most consistent/accurate with the astronomical age for the K–Pg boundary (Renne et al., in press).

Recalculation of the YTT age of Storey et al. (2012) relative to the optimisation model of Renne et al. (2010, 2011) yields 74.2 ± 0.4 ka (1 sigma, full external precision), which is within 1 sigma uncertainty of the age proposed for the YTT here. However, owing to the excess scatter (MSWD 1.9) in the full $^{40}Ar/^{39}Ar$ data of Storey et al. (2012), scatter beyond what their stated precision would suggest, we propose our age of 75.0 ± 0.9 ka to be the most accurate and robust temporal constraint for the YTT. In our experience the scatter observed in the study of Storey et al. (2012) is likely associated with: [1] dating of multi-grain aliquots of sanidine (results in improved experimental precision but significant potential for age biasing, especially as Storey et al. (2012) reject ages older and younger than their mean age and stated uncertainties) with the better approach to date single crystals only (e.g., this study) thereby permitting the screening of xenocrysts (xenocrysts up to 167 ka are evident in the study of Storey et al. (2012) and therefore in our opinion it is not suitable to fuse crystal populations), and [2] accuracy issues associated with the inter-calibration of gain and linearity of multiple ion counters when using the Noblesse noble gas mass spectrometer (e.g., Coble et al., 2011). We used a single collector configuration on a MAP 215-50 to negate these latter difficulties. Finally, whereas Storey et al. (2012) used a weighted mean calculation to determine a final age, we rely on the use of an inverse isochron that makes no assumptions about trapped $^{40}Ar/^{36}Ar$, allowing the data to define the initial trapped component. In summary, although not as precise as the age reported by Storey et al. (2012), 75.0 ± 0.9 ka is the most robust and accurate age for the YTT super eruption.

6.3. Hominin occupation of India during the Late Pleistocene

Previous analysis of sediments and ash deposits in the Son and Jurreru River valleys strongly suggested an association of the ash with the YTT event (e.g., Petraglia et al., 2007; Jones, 2010). The current $^{40}Ar/^{39}Ar$ study of the ash is the first robust chronometric study of the ash deposits in the Son and Jurreru River valleys that confirm the previous data and inferences about the age of the deposits, thus allaying criticisms that the ash could represent the OTT event (e.g., Westaway et al., 2011). The YTT ash deposits associate with Middle Palaeolithic assemblages in the Son Valley (Jones and Pal, 2009; Petraglia et al., 2012) and the Jurreru Valley (Clarkson et al., 2012; Petraglia et al., 2012). The implication is that claims for an association between Acheulean artefacts and ash (Sangode et al., 2007; Gaillard et al., 2010) are likely to be a product of redeposition and erroneous dating. While allowing for chronometric dating gaps in the Late Pleistocene of India, the presence of Middle Palaeolithic hominins between c. 77 and 38 ka implies continuity of human populations, and is thus consistent with some genetic studies which suggest a pre-Toba colonisation (Oppenheimer, 2012). In a wider sense, continuity of Middle Palaeolithic populations in India strongly suggests that hominins were not decimated by the young Toba super-eruption, thus contrasting with catastrophe theories for the near demise of humans and other hominin species (Ambrose, 1998; Williams et al., 2009; Williams, 2012a).

6.4. Evidence for forcing of Quaternary climate

The most widespread global effects of volcanic eruptions are not induced by locally devastating pyroclastic flows or ash that can penetrate the troposphere. Sulphur injected into the stratosphere during volcanic eruptions oxidises to form small droplets of sulphuric acid (i.e., sulphate aerosol, SO_4^{2-}) that decrease the amount of solar radiation reaching the surface and leads to cooling (Self, 2006). Once in the stratosphere SO_4^{2-} settles slowly under gravity into the troposphere at a rate of 35% every 8–11 months (Mather et al., 2003). SO_4^{2-} is distributed quickly by winds. For example, stratospheric SO_4^{2-} produced by the 1991 eruption of Pinatubo (Fig. 2) circled the globe in 22 days (Bluth et al., 1992). As such, records of large volcanic eruptions can potentially be preserved due to the accumulation of SO_4^{2-} in palaeoclimate archives such as ice cores (Hammer et al., 1980, 2003).

Detailed studies of the chemistry of minerals and glass in pumices from the YTT eruption enable estimation of the minimum masses of gaseous components released to earth's atmosphere during the eruption. The high eruption rate (*c.* 8×10^{12} g/s) and eruption duration (*c.* 14 days) made stratospheric venting of these gases, ash and aerosol particles likely. H_2S was the dominant sulphur-bearing species in YTT magma and it is estimated that 3.5×10^{15} g of H_2S was released to the atmosphere (Rose and Chesner, 1990). The mass of ash and gases released was nearly two orders of magnitude greater than any known historic eruption.

6.4.1. Greenland ice cores

Back (or down core) to 50 ka the chronology for the GISP2 ice core is based on the counting of annual layers (Messe et al., 1994) with the remainder of the depth–age scale based on correlation of the $\partial^{18}O$ of atmospheric O_2 records from GISP2 with the Vostock ice core, Antarctica (Sowers et al., 1993). Conservative uncertainty estimates for the period 60–80 ka are ±5 ka based on the original SPECMAP timescale and global O_2 turnover rate (Sowers et al., 1993). Within the GISP2 ice core there is evidence of a major explosive eruption during the period 60–80 ka, suggested by the distinct SO_4^{2-}, Ca^{2+} and electrical conductivity (ECM) spikes at *c.* 71 ka. Zielinski et al. (1996) suggested a correlation of this spike with the eruption of YTT (Fig. 9). Given the distance between Sumatra and Greenland, as well as dispersal models for YTT (Matthews et al., 2012), it is highly unlikely that volcanic debris (i.e., glass shards) from any Toba eruption would be found in the Greenland ice cores, but entirely plausible that aerosols were transported this distance and preserved (e.g., aerosols from the eruption of Tambora were transported a similar distance; Hammer et al., 1980). The age of the Toba YTT super-eruption and the SO_4^{2-} and ECM spike do appear to correlate in time, allowing for the large uncertainties associated with the GISP2 ice core chronology.

The climatic significance of such correlation if robust is intriguing. The SO_4^{2-} and ECM spikes occur immediately prior to a 1 ka cooling event between interstadial 20 and stadial 20 (Fig. 9) and suggest that the YTT super-eruption may have modified atmospheric conditions and forced climatic cooling on a centennial scale (Zielinski et al., 1996). However, the climate was undergoing recovery prior to the onset of stadial 20 (Fig. 9) suggesting Toba was not responsible for prolonged global cooling and onset of stadial 20. With respect to the large uncertainties associated with the GISP2 chronology beyond 50 ka, the $^{40}Ar/^{39}Ar$ age (and uncertainty) for

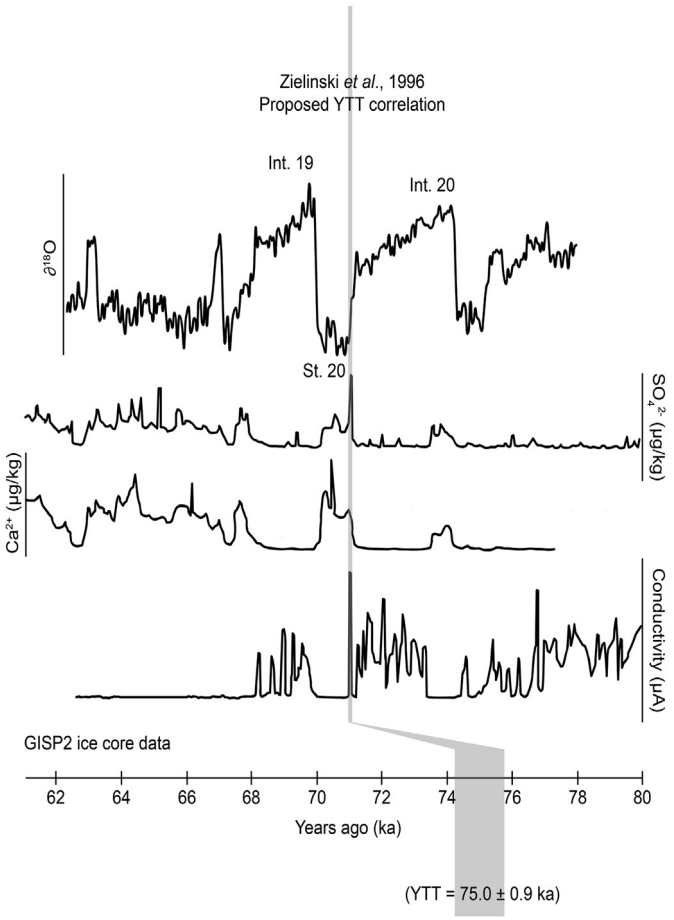

Fig. 9. GISP2 ice core data showing the proposed location of the YTT spike relative to the new high-precision $^{40}Ar/^{39}Ar$ age (75.0 ± 0.9 ka). Note short-term climatic recovery prior to the onset of stadial 20 (also shown in NGRIP ice core, see Fig. 10). Note Haslam and Petraglia (2010) show at high resolution the location of the sulphate spike in GISP 2, see their Fig. 1.

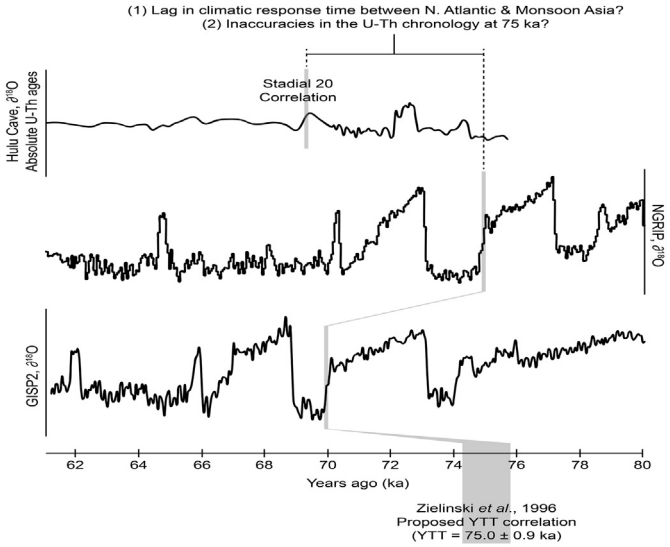

Fig. 10. Correlation of GISP 2 and NGRIP using YTT spike and onset of stadial 20, and correlation between NGRIP and Hulu Cave using the YTT age and absolute U–Th chronology. Note the 3 ka difference between the onset of stadial 20 in the North Atlantic and Monsoon Asia. $\partial^{18}O$ records are presented on the same relative scales, showing the $\partial^{18}O$ response in the ice core to be more pronounced than that of Hulu Cave.

the YTT spike in GISP2 can be utilised as an absolute time marker (Fig. 9). Further, the correlation would allow the chronologies of the multiple Greenland ice cores (e.g., GISP2 and NGRIP) to be pinned together at *c.* 75 ka (Fig. 10), beyond the *GICC05* timescale (Andersen et al., 2006), using the onset of stadial 20.

The NGRIP ice core has an annual layer counting chronology back to 60 ka (Andersen et al., 2006; Svensson et al., 2008) but pronounced annual banding in the visual stratigraphy suggests the counting-based chronology could be extended (Svensson et al., 2005). Currently, the NGRIP chronology beyond 60 ka is based on the model *ss09sea* age scale, as used in the original NGRIP publications (North Greenland Ice Core Project Members, 2004). Relative to the positions of interstadials 19 and 20, the location of the SO_4^{2-} and ECM spike in the GISP2 ice core, the onset of cooling associated with stadial 20, and the high-precision $^{40}Ar/^{39}Ar$ age for the YTT super-eruption, the chronology for NGRIP at 75 ka appears to be fairly accurate.

6.4.2. Implications for India

For India, carbon isotope work in the Middle Son Valley (at Ghoghara, Khuteli) has suggested that Toba ash was deposited on a landscape covered by C3 plants (forests) and then replaced by C4 grasslands to wooded grasslands. The identification of nearly pure C4 grassland at the top of the ash horizon was considered to be consistent with, and represent, cold temperatures due to the onset of stadial 20 following the young Toba super-eruption (Williams et al., 2009). It has been pointed out that such inferences are speculative in the absence of high-resolution deposits and precise/accurate dating (Lewis et al., 2012). This study presents a new high-precision YTT age supporting the correlation of YTT to the SO_4^{2-} and ECM spike in the GISP2 ice core and providing a tie point for linking GISP2 to NGRIP at 75 ka. The correlation casts further doubt on the validity of previous assertions about global cooling and environmental change across India coinciding with YTT and the onset of stadial 20 at *c.* 73 ka (Williams et al., 2009), i.e., the climate had deteriorated prior to the eruption of YTT at *c.* 75 ka.

6.4.3. Hulu Cave speleothem

The coincidence of the SO_4^{2-} and ECM spike with the post onset of cooling into stadial 20 and the pinning together of ice cores at 75 ka, allows us to examine the synchrony of the global onset of stadial 20 by looking at other absolutely dated palaeoclimate archives. Further, utilising other records with absolute chronologies, we can examine potential leading or lagging of the North Atlantic climate system with respect to other regions dominated by different climate systems.

High-resolution absolute dated (U–Th) Late Pleistocene monsoon records ($\partial^{18}O$) from five stalagmites from Hulu Cave near Nanjing provide a fully comparable record. Wang et al. (2001) showed good agreement between the timing of stadial 20 cooling between Hulu Cave stalagmite and the GISP2 ice core (Fig. 10) between 69 and 71 ka. However, if the correlation between the SO_4^{2-} and ECM spike with the YTT super-eruption is robust (Zielinski et al., 1996), then the new high-precision age for YTT suggests either (Fig. 10): (1) the U–Th chronology (Wang et al., 2001) for Hulu Cave stalagmite during this time period is inaccurate, or (2) with respect to different climatic systems, the North Atlantic was leading Monsoon Asia at this time. At 75 ka there is an approximate ±1 ka uncertainty associated with the Hulu Cave U–Th ages (Wang et al., 2001). Allowing for associated age uncertainties (both U–Th and $^{40}Ar/^{39}Ar$), there is currently a *c.* 3 ka offset in the onset of stadial 20 between the North Atlantic and Monsoon Asia. Further effort to resolve the 3 ka offset (either with respect to inaccuracies

in dating or to the lagging of the Monsoon Asia climate system) is required.

Although other records extend back beyond 75 ka, e.g., Lake Suigetsu (Nakagawa et al., 2003; Smith et al., 2011b), Cariaco Basin marine core (Hughen et al., 2004), Monticchio lake core (Watts et al., 1996), the notable absence of absolute chronologies for the appropriate time periods prevents correlation to the Greenland ice cores and Hulu cave at 75 ka, and thus restricts resolution of further sequences of climatic events that may test the two hypotheses proposed above.

6.4.4. Antarctic ice cores

The link between the Greenland and Antarctic ice cores is already fairly well constrained by the matching (tuning) of methane records (EPICA Community Members, 2006). However, there is still some uncertainty in the tuning of ice cores from the two hemispheres due to offset in the age of ice and air bubbles in the ice cores. The identification of a direct Toba tie point would enable correlation (rather than tuning) of records revealing the degree of synchronicity of inter-hemispheric climate around 75 ka. To the best of our knowledge a definitive Toba signal, beyond increased dust content between 70 and 75 ka (EPICA community members, 2004), has not been located within the Antarctic ice cores. Effort to locate a YTT signal in the Antarctic ice cores could prove fruitful.

6.5. Dating of ultra-distal tephra deposits

Acknowledging the issues associate with $^{40}Ar/^{39}Ar$ dating of volcanic glass shards (Morgan et al., 2009), we focussed on the dating of distal biotite shards, obtaining statistically robust and reproducible $^{40}Ar/^{39}Ar$ ages. The approach developed for dating of ultra-distal tephra deposits has great potential for tephrostratigraphy and tephrochronology (Lowe, 2011), allowing correlation of isochronous stratigraphic markers across continents when dissection by geochemical techniques becomes problematic. With the continued development of highly-sensitive multi-collector noble gas mass spectrometers (e.g., Mark et al., 2009; Coble et al., 2011) that allow for dating of ever decreasing sample sizes, and the refinement of sample irradiation protocols (e.g., the use of deuteron–deuteron fusion neutrons; Renne et al., 2005), achievable precision and hence stratigraphic resolution will improve.

7. Conclusions

The study has yielded a high-precision $^{40}Ar/^{39}Ar$ age for the young Toba super-eruption: 75.0 ± 0.9 ka (1 sigma, relative to Renne et al., (2010, 2011), full external precision). We have developed an approach for the dating of ultra-distal tephra using the $^{40}Ar/^{39}Ar$ technique by targeting small shards of biotite. Sample preparation of sub-100 μm shards of biotite is difficult (and tedious) but in this case the biotite crystal populations have yielded sufficiently precise (*c.* ± 5%) and reproducible $^{40}Ar/^{39}Ar$ ages to allow establishment of tephra provenance. The $^{40}Ar/^{39}Ar$ age data presented here show that the primary air-fall tephra layers in the Middle Son Valley and Jurreru Valley correlate with the YTT, demonstrating that air-fall deposits blanketed northern and southern India, with the expectation that Middle Palaeolithic hominins associate with the super-eruption. The study supports the conclusion that the young Toba super-eruption was not responsible for the onset of stadial 20, but the 75 ka eruption occurred post onset of the climatic cooling, as highlighted by Haslam and Petraglia (2010). The YTT and its high-precision $^{40}Ar/^{39}Ar$ age can serve as a tie point for linking of the multiple Greenland ice cores beyond the *GICC05* timescale, and permits correlation to other absolutely dated palaeoclimate archives for the testing of synchronicity in the response of the global climate system. The identification of a Toba signal in the Antarctic ice cores would allow for inter-hemispheric correlation of climate records.

Acknowledgements

A NERC Services & Facilities Grant IP/1185/0510 supported the laboratory work. NERC are thanked for continued funding of the Argon Isotope Facility at SUERC. The Archaeological Survey of India provided permits for the Indian fieldwork and sample analyses. The Leverhulme Trust and the British Academy provided field funding. For fieldwork and sample collection, we wish to thank the large interdisciplinary teams for their efforts, including James Blinkhorn, Pete Ditchfield, Adam Durant, Emma Gatti, Michael Haslam, Sacha Jones, Naomi Matthews, and Christina Neudorf. Jim Imlach and Ross Dymock (SUERC) are thanked for assistance with tedious sample preparation. Prof. Tony Fallick (SUERC), Prof. Chris Bronk-Ramsey (Oxford University), Prof. John Lowe (Royal Holloway) and Prof. Takeshi Nakagawa (Newcastle University) are thanked for discussion. Brad Singer is thanked for editorial handling and constructive comments. Terry Spell is thanked for a thorough review which helped improve the quality of this contribution.

Editorial handling by: B. Singer

Appendix A. Supplementary data

Supplementary data related to this article can be found at http://dx.doi.org/10.1016/j.quageo.2012.12.004.

References

Acharyya, S.K., Basu, P.K., 1993. Toba ash on the Indian subcontinent and its implications for correlation of late Pleistocene alluvium. Quaternary Research 40, 10–19.

Ambrose, S.H., 1998. Late Pleistocene human bottlenecks, volcanic winter, and differentiation of modern humans. Journal of Human Evolution 34, 623–651.

Andersen, K.K., Svensson, A., Johnsen, S.J., Rasmussen, S.O., Bigler, M., Rothlisberger, R., Ruth, U., Siggard-Andersen, M.L., Steffensen, J.P., Dahl-Jensen, D., Vinther, B.M., Clausen, H.B., 2006. Greenland ice core chronology 2005, 15-42 ka. Part 1: constructing the time scale. Quaternary Science Reviews 25, 3246–3255.

Balter, M., 2010. Of two minds about Toba's impact. Science 327, 1187–1188.

Blinkhorn, J., Bora, J., Koshy, J., Korisettar, R., Boivin, N., Petraglia, M., 2010. Systematic transect survey enhances the investigation of rock art in its landscape: an example from the Katavani Kunta Valley, Kurnool District. Man and Environment 34 (2), 1–12.

Blinkhorn, J., Parker, A.G., Ditchfield, P., Haslam, M., Petraglia, M., 2012. Uncovering a landscape buried by the super-eruption of Toba, 74,000 years ago: a multi-proxy environmental reconstruction of landscape heterogeneity in the Jurreru Valley, South India. Quaternary International 258, 135–147.

Bluth, G.J.S., Doiron, S.D., Schnetzler, C.C., Krueger, A.J., Walter, L.S., 1992. Global tracking of the SO_2 clouds from the June 1991 Mount Pinatubo eruptions. Geophysical Research Letters 19, 151–154.

Bowler, J.M., Johnston, H., Olley, J.M., Prescott, J.R., Roberts, R.G., Shawcross, W., Spooner, N.A., 2003. New ages for human occupation and climatic change at Lake Mungo, Australia. Nature 421, 837–840.

Carey, S., Sigurdsson, H., Mandeville, C., Bronto, S., 1996. Pyroclastic flows and surges over water: an example from the 1883 Krakatau eruption. Bulletin of Volcanology 57, 493–511.

Chesner, C.A., Rose, W.I., 1991. Stratigraphy of the Toba tuffs and evolution of the Toba Caldera Complex, Sumatra, Indonesia. Bulletin of Volcanology 53, 343–356.

Chesner, C.A., Rose, W.I., Drake, A.D.R., Westgate, J.A., 1991. Eruptive history of Earth's largest Quaternary caldera (Toba, Indonesia) clarified. Geology 19, 200–203.

Chesner, C.A., 1998. Petrogenesis of the Toba tuffs, Sumatra, Indonesia. Journal of Petrology 39, 397–438.

Clarkson, C., Jones, S., Harris, C., 2012. Continuity and change in the lithic industries of the Jurreru Valley, India, before and after the Toba eruption. Quaternary International 258, 165–179.

Coble, M.A., Grove, M., Calvert, A.T., 2011. Calibration of Nu-instruments Noblesse multicollector mass spectrometers for argon isotopic measurements using a newly developed reference gas. Chemical Geology 290, 75–87.

Cohen, A.S., Stone, J.R., Beuning, K.R.M., Park, L.E., Reinthal, P.N., Dettman, D., Scholz, C.A., Johnson, T.C., King, J.W., Talbot, M.R., Brown, E.T., Ivory, S.J., 2007. Ecological consequences of early Late Pleistocene megadroughts in tropical Africa. Proceedings of the National Academy of Sciences of the United States of America 104, 16422–16437.

Ellis, B.S., Mark, D.F., Pritchard, C.J., Wolff, J.A., 2012. Temporal dissection of the Huckleberry Ridge Tuff using the $^{40}Ar/^{39}Ar$ dating technique. Quaternary Geochronology 9, 34–41.

EPICA community members (Augustin et al.,), 2004. Eight glacial cycles from an Antarctic ice core. Nature 429, 623–628.

EPICA community members (Fischer et al.,), 2006. One to one coupling of glacial climate variability in Greenland and Antarctica. Nature 444, 195–198.

Gaillard, C., Mishra, S., Singh, M., Deo, S., Abbas, R., 2010. Lower and early Middle Pleistocene Acheulian in the Indian sub-continent. Quaternary International 223–224, 234–241.

Gathorne-Hardy, F.J., Harcourt-Smith, W.E.H., 2003. The super-eruption of Toba, did it cause a human bottleneck? Journal of Human Evolution 45, 227–230.

Gatti, E., Durant, A.J., Gibbard, P.L., Oppenheimer, C., 2011. Youngest Toba tuff in the Son Valley, India: a weak and discontinuous stratigraphic marker. Quaternary Science Reviews 30, 3925–3935.

Haigh, J., Maynard Smith, J., 1972. Population size and protein variation in man. Genetical Research 19, 73–89.

Hammer, C.U., Claussen, H.B., Dansgaard, W., 1980. Greenland ice sheet evidence of post-glacial volcanism and its climatic impact. Nature 288, 230–235.

Hammer et al., C.U., Kurat, G., Hoppe, P., Grum, W., Clausen, H.B., 2003. Thera eruption date 1645 BC confirmed by new ice core data? In: Bietak, M. (Ed.), The Synchronisation of Civilisations in the Eastern Mediterranean in the Second Millennium B.C. II, pp. 87–94.

Harpending, H.C., Sherry, S.T., Rogers, A.L., Stoneking, M., 1993. The genetic structure of ancient human populations. Current Anthropology 34, 483–496.

Haslam, M., Petraglia, M., 2010. Comment on 'Environmental impact of the 73 ka Toba super-eruption in South Asia' by M.A.J. Williams, S.H. Ambrose, S. van der Kaars, C. Ruehlemann, U. Chattopadhyaya, J. Pal & P.R. Chauhan [Palaeogeography, Palaeoclimatology, Palaeoecology, 284 (2009) 295-314]. Paleogeography, Palaeoclimatology, Palaeoecology 296, 199–203.

Haslam, M., Clarkson, C., Roberts, R.G., Bora, J., Korisettar, R., Ditchfield, P., Chivas, A., Harris, C., Smith, V., Oh, A., Eksambekar, S., Boivin, N., Petraglia, M., 2012. A southern Indian Middle Palaeolithic occupation surface sealed by the 74 ka Toba eruption: further evidence from Jwalapuram Locality 22. Quaternary International 258, 191–199.

Hildreth, W., Wilson, C.J.N., 2007. Compositional zoning of the Bishop Tuff. Journal of Petrology 48, 951–999.

Hora, J.M., Singer, B.S., Jicha, B.R., Beard, B.L., Johnson, C.M., de Silva, S., Salisbury, M., 2010. Volcanic biotite-sanidine $^{40}Ar/^{39}Ar$ age discordances reflect Ar partitioning and pre-eruption closure in biotite. Geology 38, 923–926.

Hughen, K., Lehman, S., Southon, J., Overpeck, J., Marchal, O., Herring, C., Turnbull, J., 2004. 14C activity and global carbon cycle changes over the past 50,000 years. Science 303, 202–207.

Hynek, S.A., Brown, F.H., Fernandez, D.P., 2010. A rapid method for hand picking potassium-rich feldspar from silicic tephra. Quaternary Geochronology 6, 285–288.

Jones, S.C., 2007. The Toba super-volcanic eruption: tephra-fall deposits in India and paleoanthropological implications. In: Petraglia, M.D., Allchin, B. (Eds.), The Evolution and History of Human Populations in South Asia, pp. 173–200.

Jones, S., Pal, J.N., 2009. The Palaeolithic of the Middle Son Valley, north-central India: changes in hominin lithic technology and behaviour during the Upper Pleistocene. Journal of Anthropological Archaeology 28, 323–341.

Jones, S., 2010. Palaeoenvironmental response to the 74 ka Toba ash-fall in the Jurreru and Middle Son Valleys in southern and north-central India. Quaternary Research 73, 36–350.

Jorde, L.B., Ba, shad, M., Rogers, A.R., 1998. Using mitochondrial and nuclear DNA markers to reconstruct human evolution. BioEssays 20, 126–136.

Knight, M.D., Walker, G.P.L., Ellwood, B.B., Diehl, J.F., 1986. Stratigraphy, palaeomagnetism and magnetic fabric of the Toba tuffs: constraints on the sources and eruptive styles. Journal of Geophysical Research B91 (10), 382. 355–410.

Kuiper, K.F., Deino, A., Hilgen, F.J., Krijgsman, W., Renne, P.R., Wijbrans, J.R., 2008. Synchronizing rock clocks of earth history. Science 25 (320), 500–504.

Lee, M.Y., Chen, C.H., Wei, K.Y., Lizuka, Y., Carey, S., 2004. First Toba super-eruption revival. Geology 32, 61–64.

Lee, J.-L., Marti, K., Severinghaus, J.P., Kawamura, K., Yoo, H.-S., Lee, J.B., Kim, J.S., 2006. A redetermination of the isotopic abundances of atmospheric Ar. Geochimica et Cosmochimica Acta 70, 4507–4512.

Lewis, L., Ditchfield, P., Pal, J.N., Petraglia, M., 2012. Grain size distribution analysis of sediments containing Younger Toba tephra from Ghoghara, Middle Son Valley, India. Quaternary International 258, 180–190.

Lowe, D.J., 2011. Tephrochronology and its application: a review. Quaternary Geochronology 6, 107–153.

Louys, J., 2012. Mammal community structure of Sudanese fossil assemblages from the Late Pleistocene, and a discussion on the ecological effects of the Toba eruption. Quaternary International 258, 80–87.

Mark, D.F., Barfod, D., Stuart, F.M., Imlach, J., 2009. The ARGUS multicollector noble gas mass spectrometer: performance for $^{40}Ar/^{39}Ar$ geochronology. Geochemistry, Geophysics, Geosystems 10, 1–9.

Mark, D.F., Gonzalez, S., Huddart, D., Bohnel, H., 2010. Dating of the Valsequillo volcanic deposits: resolution of an ongoing controversy in Central Mexico. Journal of Human Evolution 58, 441–445.

Mark, D.F., Rice, C.M., Lee, M.R., Fallick, A.E., Boyce, A., Trewin, N.H., Lee, J.K.W., 2011a. $^{40}Ar/^{39}Ar$ dating of hydrothermal activity, biota and gold mineralization in the Rhynie hot-spring system, Aberdeenshire, Scotland. Geochimica et Cosmochimica Acta 75, 555–569.

Mark, D.F., Stuart, F.M., de Podesta, M., 2011b. New high-precision measurements of the isotopic composition of atmospheric argon. Geochimica et Cosmochimica Acta 75, 7494–7501.

Mason, B.G., Pyle, D.M., oppenheimer, C., 2004. The size and frequency of the largest explosive eruptions on Earth. Bulletin of Volcanology 66, 735–748.

Mather, T.A., Pyle, D.M., Oppenheimer, C., 2003. Tropospheric Volcanic Aerosol. In: Volcanism and the Earth's Atmosphere, Geophysical Monograph, vol. 139. AGU.

Matthews, N.E., Smith, V.C., Costa, A., Durant, A.J., Pyle, D.M., Pearce, N.J.G., 2012. Ultra-distal tephra deposits from super-eruptions: examples from Toba and New Zealand. Quaternary International 258, 54–79.

Messe, D.A., Gow, A.J., Grootes, P.M., Mayweski, P.A., Ram, M., Stuvier, M., Taylor, K.C., Waddington, E.D., Zielinski, G.A., 1994. The accumulation record from the GISP2 core as an indicator of climate change throughout the Holocene. Science 266, 1680–1682.

Mishra, S., Rajaguru, S.N., 1994. Comment on 'Toba ash on the Indian subcontinent and its implication for the correlation of Late Pleistocene alluvium'. Quaternary Research 41, 396–397.

Morgan, L.M., Renne, P.R., Taylor, R.E., WoldeGabriel, G., 2009. Archaeological age constraints from eruption ages of obsidian: examples from the Middle Awash, Ethiopia. Quaternary Geochronology 4 (4), 288–298.

Nakagawa, T., Kitagawa, H., Yasuda, Y., Tarasov, P.E., Nishida, K., Gotanda, K., Sawai, Y., Yangtze River Civilization Project Members, 2003. Asynchronous climate changes in the North Atlantic and Japan during the last termination. Science 299, 688–691.

Neudorf, C.M., Roberts, R.G., Jacobs, Z., 2012. Sources of overdispersion in a K-rich feldspar sample from north-central India: insights from De, K content and IRSL age distributions for individual grains. Radiation Measurements 47, 696–702.

Ninkovich, D., Shackleton, N.J., Abdel-Monem, A.A., Obradovich, J.D., Izett, G.K., 1978. K-Ar age of the late Pleistocene eruption of Toba, north Sumatra. Nature 276, 574–577.

Ninkovich, D., 1979. Distribution, age and chemical composition of tephra layers in deep sea sediments off western Indonesia. Journal of Geothermal Research 5, 67–86.

Nomade, S., Renne, P.R., Vogel, N., Deino, A.L., Sharp, W.D., Becker, T.A., Jaouni, A.R., Mundil, R., 2005. Alder Creek sanidine (ACs-2): a Quaternary $^{40}Ar/^{39}Ar$ dating standard tied to the Cobb Mountain geomagnetic event. Chemical Geology 218, 315–338.

North Greenland Ice Core Project Members, 2004. High resolution record of northern hemispheric climate extending into the last interglacial period. Nature 431, 147–151.

Oppenheimer, C., 2002. Limited global change due to the largest known Quaternary eruption, Toba ~74 kyr BP? Quaternary Science Reviews 81, 1593–1609.

Oppenheimer, S., 2012. A single southern exit of modern humans from Africa: before or after Toba? Quaternary International 258, 88–99.

Paine, J.H., Nomade, S., Renne, P.R., 2006. Quantification of ^{39}Ar recoil ejection from GA1550 biotite during neutron irradiation as a function of grain dimensions. Geochimica et Cosmochimica Acta 70, 1507–1517.

Pattan, J.N., Shane, P., Pearce, N.J.G., Banakar, V.K., Parthiban, G., 2001. An occurrence of ~74 ka youngest Toba tephra from western continental margin of India. Current Science 80, 1322–1326.

Petraglia, M., Korisettar, R., Boivin, N., Clarkson, C., Ditchfield, P., Jones, S., Koshy, J., Lahr, M.M., Oppenheimer, C., Pyle, D., Roberts, R., Schwenninger, J.-L., Arnold, L., White, K., 2007. Middle Palaeolithic assemblages from the Indian subcontinent before and after the Toba super-eruption. Science 317, 114–116.

Petraglia, M.D., Ditchfield, P., Jones, S., Korisettar, R., Pal, J.N., 2012. The Toba volcanic super-eruption, environmental change, and hominin occupation history in India over the last 140,000 years. Quaternary International 258, 119–134.

Rampino, M.R., Ambrose, S.H., 2000. In: McCoy, F.W., Heiken, G. (Eds.), Volcanic Hazards and Disasters in Human Antiquity, Geological Society of America Special Paper 345, Boulder, pp. 71–82.

Rampino, M.R., Self, S., 1993. Climate-Volcanism feedback and the Toba eruption of 74,000 years ago. Quaternary Research 40, 269–280.

Rampino, M.R., Self, S., 1992. Volcanic winter and accelerated glaciation following the Toba super-eruption. Nature 359, 50–52.

Renne, P.R., Swisher, C.C., Deino, A.L., Karner, D.B., Owens, T.L., DePaolo, D.J., 1998. Intercalibration of standards, absolute ages and uncertainties in $^{40}Ar/^{39}Ar$ dating. Chemical Geology 145, 117–152.

Renne, P.R., Deino, A.L., Hames, W.E., Heizler, M.T., Hemming, S.R., Hodges, K.V., Koppers, A.A.P., Mark, D.F., Morgan, L.E., Phillips, D., Singer, B.S., Turring, B.D., Villa, I.M., Villeneuve, M., Wijbrans, R.R., 2009. Data reporting norms for $^{40}Ar/^{39}Ar$ geochronology. Quaternary Geochronology, 346–352.

Renne, P.R., Knight, K.B., Nomade, S., Leung, K.N., Lou, T.P., 2005. Application of deuteron-deuteron (D-D) fusion neutrons to $^{40}Ar/^{39}Ar$ geochronology. Applied Radiation and Isotopes 62, 25–32.

Renne, P.R., Mundil, R., Balco, G., Min, K., Ludwig, K.R., 2010. Joint determination of ^{40}K decay constants and $^{40}Ar^*/^{40}K$ for the Fish Canyon sanidine standard, and improved accuracy for $^{40}Ar/^{39}Ar$ geochronology. Geochimica et Cosmochimica Acta 74, 5349–5367.

Renne, P.R., Balco, G., Ludwig, K.R., Mundil, R., Min, K., 2011. Response to the comment by W.H. Schwarz et al. on "Joint determination of ^{40}K decay constants and ^{40}Ar*/^{40}K for the Fish Canyon sanidine standard, and improved accuracy for ^{40}Ar/^{39}Ar geochronology" by P.R. Renne et al., 2010. Geochimica et Cosmochimica Acta 75, 5097–5100.

Renne, P.R., Deino, A.L., Hilgen, F.J., Kuiper, K.F., Mark, D.F., Mitchell III, W.S., Morgan, L.E., Mundil, R., Smit, J. Timescales of critical events around the Cretaceous-Paleogene boundary. Science., in press.

Richter, D., tostevin, G., Skrdla, P., 2008. Bohuncian technology and thermoluminescence dating of the type locality of Brno-Bohunice (Czech Republic). Journal of Human Evolution 55, 871–885.

Rivera, T.A., Storey, M., Zeeden, C., Hilgen, F.J., Kuiper, K., 2011. A refined astronomically calibrated ^{40}Ar/^{39}Ar age for Fish Canyon sanidine. Earth and Planetary Science Letters 311, 420–426.

Roberts, R., Fenwick, J., Arnold, L., Jacobs, Z., Jafari, Y., 2010, Numerical Dating of Sediments Associated with Volcanic Ash and Stone Artefacts in Southern and Northeastern India. Paper Presented at the Toba Super-Eruption Conference, University of Oxford, 20 February 2010.

Rose, W.I., Chesner, C.A., 1990. Worldwide dispersal of ash and gases from earth's largest known eruption: Toba, Sumatra, 75 ka. Paleogeography, Palaeoclimatology, Palaeoecology 89, 269–275.

Sangode, S.S., Mishra, S., Naik, S., Deo, S., 2007. Magnetostratigraphy of the Quaternary sediments associated with some Toba Tephra and Acheulian artefact bearing localities in the western and central India. Gondwana Magazine special volume 10, 111–121.

Sarna-Wojcicki, A.M., Shipley, S., Waitt Jr., R.B., Dzurisin, D., Wood, S.H., Lipman, P.W., Mullineaux, D.R., 1981. In: Lipman, P.W., Mullineaux, D.R. (Eds.), Areal Distribution, Thickness, Mass, Volume, and Grain Size of Air-fall Ash from the Six Major Eruptions of 1980, U.S. Geological Survey Professional Paper, 1250, pp. 577–600.

Scholz, C.A., Johnson, T.C., Cohen, A.S., King, J.W., Peck, J.A., Overpeck, J.T., Talbot, M.R., Brown, E.T., Kaleindekafe, L., Amoako, P.Y.O., Lyons, R.P., Shanahan, T.M., Castaneda, I.S., Heil, C.W., Forman, S.I., McHague, L.R., Beuning, K.R., Gomez, J., Pierson, J., 2007. East African megadroughts between 135 and 75 thousand years ago and bearing on modern human origins. Proceedings of the National Academy of Sciences of the United States of America 104, 16416–16421.

Schulz, H., Emeis, K.Ch., Erlenkeuser, H., Von Rad, U., Rolf, Ch, 2002. The Toba volcanic event and interstadial/stadial climates at the marine isotopic stage 5 to 4 transition in the Northern Indian Ocean. Quaternary Research 57, 22–31.

Scrivenor, J.B., 1930. A recent rhyolite ash with sponge spicules and diatoms in Malaya. Geological Magazine LXVII, 385–393.

Scott, W.E., Hoblitt, R.P., Torres, R.C., Self, S., Martinez, M.M.L., Timoteo Jr., N., 1996. Pyroclastic flos of the June 15, 1991, climactic eruption of Mount Pinatubo. In: Newhall, C.G., Punongbayan, R.S. (Eds.), Fire and Mud, Eruptions and Lahars of Mount Pinatubo, Phillipines. Phillipine Institute of Volcanology and Seismology and University of Washington, pp. 545–570.

Self, S., 2006. The effects and consequences of very large explosive volcanic eruptions. Philosophical Transactions of the Royal Society 364, 2073–2097.

Self, S., Gertissler, R., Thordarson, T., Rampino, M.R., Wolff, J.A., 2004. Magma volume, volatile emissions, and stratospheric aerosols from the 1815 eruption of Tambora. Geophysical Research Letters 31, L20608. http://dx.doi.org/10.1029/2004GL020925.

Sharma, G.R., Clark, J.D., 1983. Palaeoenvironments and Prehistory in the Middle Son Valley. Abinash Prakashan, Allahbad.

Shipton, C., Bora, J., Koshy, J., Petraglia, M., Haslam, M., Korisettar, R., 2010. Systematic transect survey of the Jurreru valley, Andhra Pradesh. Man and Environment 35, 24–36.

Smith, V.C., Pearce, N.J.G., Matthews, N.E., Westgate, J.A., Petraglia, M.D., Haslam, M., Lane, C.S., Korisettar, R., Pal, J.N., 2011a. Geochemical fingerprinting the widespread Toba tephra using biotite compositions. Quaternary International 246, 97–104.

Smith, V.C., Mark, D.F., Staff, R.A., Blockley, S.P.E., Bronk-Ramsey, C., Bryant, C.L., Nakagawa, T., Han, K.K., Weh, A., Takemura, K., Danhara, T., Suigtsu 2006 Project Members, 2011b. Toward establishing precise ^{40}Ar/^{39}Ar chronologies for Late Pleistocene palaeoclimate archives: an example from the Lake Suigetsu (Japan) sedimentary record. Quaternary Science Reviews 30, 2845–2850.

Sowers, T., Bender, M., Labeyrie, L., Martinson, D., Jouzel, J., Raynaud, D., Pichon, J.J., Korotkevich, Y.S., 1993. A 135,000-year Vostok-SPECMAP Common temporal framework. Paleoceanography 8 (6), 737.

Steiger, R.H., Jäger, E., 1977. Subcommission on geochronology: convention on the use of decay constants in geo- and cosmochronology. Earth and Planetary Science Letters 36, 359–362.

Storey, M., Roberts, R.G., Saidin, M., 2012. Astronomically calibrated ^{40}Ar/^{39}Ar age for the Toba supereruption and global synchronization of late Quaternary records. Proceedings of the National Academy of Sciences of the United States of America. http://dx.doi.org/10.1073/pnas.1208178109.

Svensson, A., Nielsen, S.W., Kipfstuhl, S., Johnsen, S.J., Steffensen, J.P., Bigler, M., Ruth, U., Rothlisberger, R., 2005. Visual stratigraphy of the North Greenland Ice Core Project (NorthGRIP) ice core during the last glacial period. Journal of Geophysical Research 110, D02108.

Svensson, A., Andersen, K.K., Bigler, M., Clausen, H.B., Dahl-Jensen, D., Davies, S.M., Johnsen, S.J., Muscheler, R., Parrenin, F., Rasmussen, S.O., Rothlisberger, R., Seierstad, I., Steffensen, J.P., Vinther, B.M., 2008. A 60,000 year Greenland stratigraphic ice core chronology. Climate of the Past 4, 47–57.

Tishkoff, S.A., Reed, F.A., Friedlaender, F.R., Ehret, C., Ranciaro, A., Froment, A., Hirbo, J.B., Awomoyi, A.A., Bodo, J.-M., Doumbo, O., Ibrahim, M., Juma, A.T., Kotze, M.J., Lema, G., Moore, J.H., Mortensen, H., Nyambo, T.B., Omar, S.A., Powell, K., Pretorius, G.S., Smith, M.W., Thera, M.A., Wambebe, C., Weber, J.L., Williams, S.M., 2009. The genetic structure and history of Africans and African Americans. Science 324, 1035–1044.

Vanlaningham, S., Mark, D.F., 2011. Step heating of ^{40}Ar/^{39}Ar standard mineral mixtures: Investigation of a fine-grained bulk sediment provenance tool. Geochimica et Cosmochimica Acta 75, 2324–2335.

Wang, Y.J., Cheng, H., Edwards, R.L., An, Z.S., Wu, J.Y., Shen, C.C., Dorale, J.A., 2001. A high-resolution absolute-dated late Pleistocene monsoon record from Hulu Cave, China. Science 294, 2345–2348.

Watts, W.A., Allen, J.R.M., Huntley, B., 1996. Vegetation history and climate of the last glacial period at Lago Grande di Monticchio, southern Italy. Quaternary Science Reviews 15, 133–153.

Westaway, R., Mishra, S., Deo, S., Bridgland, D.R., 2011. Methods for determination of the age of Pleistocene tephra, derived from eruption of Toba, in central India. Journal of Earth System Science 120 (3), 503–530.

Westgate, J., Shane, P., Pearce, N., Perkins, W., Korisettar, R., Chesner, C., Williams, M., Acharyya, S.K., 1998. All Toba tephra occurrences across peninsular India belong to the 75,000 years B.P. eruption. Quaternary Research 50, 107–112.

Williams, M., Pal, J.N., Jaiswal, M., Singhvi, A.K., 2006. River response to Quaternary climatic fluctuations: evidence from the Son and Belan valleys, north-central India. Quaternary Science Reviews 25, 2619–2631.

Williams, M., Ambrose, S.H., van der Kaars, S., Ruehlemann, C., Chattopadhyaya, U.C., Pal, J.N., Chauhan, P., 2009. Environmental impact of the 73 ka Toba super-eruption in South Asia. Paleogeography, Palaeoclimatology, Palaeoecology 284, 295–314.

Williams, M., 2012a. Did the 73 ka Toba super-eruption have an enduring effect? Insights from genetics, prehistoric archaeology, pollen analysis, stable isotope geochemistry, geomorphology, ice cores and climate models. Quaternary International 269, 87–93.

Williams, M., 2012b. The ~73 ka Toba super-eruption and its impact: history of a debate. Quaternary International 258, 19–29.

Yokoyama, T., Hehanussa, P.E., 1981. The Age of 'Old Toba Tuff' and Some Problems on the Geohistory of Lake Toba, Sumatra, Indonesia. In: Paleolimnology of Lake Biwa and the Japanese Pleistocene, vol. 9, pp. 177–186.

Zielinski, G.A., Mayewski, P.A., Meeker, L.D., Whitlow, S., Twickler, M.S., 1996. Potential atmospheric impact of the Toba mega-eruption ~71,000 years ago. Geophysical Research Letters 23, 837–840.